HOKKAIDO UNIVERSITY

Title	Magnetic and electrical properties of quadruple perovskites with 12 layer structures Ba4LnM3O12 (Ln=rare earths; M=Ru, Ir) : The role of metal-metal bonding in perovskite-related oxides
Author(s)	Shimoda, Yuki; Doi, Yoshihiro; Wakeshima, Makoto et al.
Citation	Journal of Solid State Chemistry, 183(9), 1962-1969 https://doi.org/10.1016/j.jssc.2010.06.023
Issue Date	2010-09
Doc URL	https://hdl.handle.net/2115/44030
Type	journal article
File Information	JSSC183-9_1962-1969.pdf

Magnetic and Electrical Properties of Quadruple Perovskites with

12 Layer Structures Ba$_4$$Ln$$M_3O_{12}$ (Ln = Rare Earths; M = Ru, Ir) :

The Role of Metal-Metal Bonding in Perovskite-Related Oxides

Yuki Shimoda, Yoshihiro Doi, Makoto Wakeshima and Yukio Hinatsu

Division of Chemistry, Hokkaido University, Sapporo 060-0810, Japan

Abstract

Structures and magnetic and electrical properties of quadruple perovskites containing rare earths $Ba_4LnM_3O_{12}$ (Ln = rare earths; M = Ru, Ir) were investigated. They crystallize in the 12L-perovskite-type structure. Three MO_6 octahedra are connected to each other by face-sharing and form a M_3O_{12} trimer. The M_3O_{12} trimers and LnO_6 octahedra are alternately linked by corner-sharing, forming the perovskite-type structure with 12 layers. For Ln = Ce, Pr , and Tb, both the Ln and M ions are in the tetravalent state ($Ba_4Ln^{4+}M^{4+}_3O_{12}$), and for other Ln ions, Ln ions are in the trivalent state and the mean oxidation state of M ions is +4.33 ($Ba_4Ln^{3+}M^{4.33+}_3O_{12}$). All the $Ba_4Ln^{3+}Ru^{4.33+}_3O_{12}$ compounds show magnetic ordering at low temperatures, while any of the corresponding iridium-containing compounds $Ba_4Ln^{3+}Ir^{4.33+}_3O_{12}$ is paramagnetic down to 1.8 K. $Ba_4Ce^{4+}Ir^{4+}_3O_{12}$ orders antiferromagnetically at 10.5 K, while the corresponding ruthenium-containing compound $Ba_4Ce^{4+}Ru^{4+}_3O_{12}$ is paramagnetic. These magnetic results were well understood by the magnetic behavior of M_3O_{12}. The effective magnetic moments and the entropy change for the magnetic ordering show that the trimers $Ru^{4.33+}_3O_{12}$ and $Ir^{4+}_3O_{12}$ have the $S = 1/2$ ground state, and in other cases there is no magnetic contribution from the trimers $Ru^{4+}_3O_{12}$ or $Ir^{4.33+}_3O_{12}$.

Measurements of the electrical resistivity of $Ba_4LnM_3O_{12}$ and its analysis show that these compounds demonstrate two-dimensional Mott-variable range hopping behavior.

1. Introduction

Perovskite-type oxides have the general formula ABO_3, in which A represents a large metal cation and B represents a small one. Structures of perovskite compounds can be regarded as the stacking of close-packed AO_3 layers and the filling of subsequent octahedral sites by B site ions. The difference in the stacking sequence changes the way of linkage of BO_6 octahedra: the corner-sharing BO_6 in the cubic perovskite (3L: three-layer) with $abc...$ sequence, the face-sharing BO_6 in 2L-perovskite (2L: two-layer) with $ab...$ sequence, and mixed linkages between the corner- and face-sharing in various intergrowth structures [1].

The rare earth ion is relatively large and tends to adopt a high coordination number. Therefore, the rare earth ion usually sits at the A site of the perovskite oxides ABO_3, and does not much contribute to their magnetic properties. By selecting large alkaline earth elements such as Sr and Ba as the A site atoms, one can accommodate the rare earth (Ln) with smaller transition elements (M) at the B sites. Many researchers have been interested in the properties of the perovskites containing pentavalent ruthenium and iridium ions. Such highly oxidized cations from the second and third transition series sometimes show quite unusual magnetic behavior.

The stacking sequence is controlled by changing the ratio of the Ln and M ions. Double perovskites Ba_2LnMO_6 are formed (doubling the formula unit, Fig. 1 (a)), when the size and/or charge of the Ln and M cations are sufficiently different. The Ln and M ions are regularly ordered over the six-coordinate B sites. These compounds show antiferromagnetic transitions at low temperatures [2-26], and the Neel temperatures for Ba_2LnRuO_6 compounds change widely from 26 to 117 K [14, 15]. This feature is affected by the properties of Ln ions.

When the ratio of Ln:M is 1:2, triple perovskites $Ba_3LnM_2O_9$ are formed (Fig. 1 (c)). Two MO_6 octahedra are connected by face-sharing and form a M_2O_9 dimer. These dimers and LnO_6 octahedra are placed alternately; thus, 6-layer (6L) structure is generated (the stacking sequence: $abacbc...$). Magnetic properties of these compounds have been investigated [27-53]. In the $Ba_3LnM_2O_9$, the ground state of the total spin of the isolated M_2O_9 dimer may be zero,

i.e., $S_{dimer} = S_1 + S_2 = 0$, for the case that the antiferromagnetic coupling exists between the M ions.

Now, we started studies on quadruple perovskites $Ba_4LnM_3O_{12}$ in which the ratio of Ln:M is 1:3. Three MO_6 octahedra are connected to each other by face-sharing and form a M_3O_{12} trimer. The M_3O_{12} trimers and LnO_6 octahedra are alternately linked by corner-sharing (Fig. 1 (d)). As shown in this figure, the perovskite-type structure with 12 layers is formed (the stacking sequence: *ababcacabcbc*...) [54-58]. In this case, the total magnetic moment of the M_3O_{12} trimer does not disappear as far as three M ions are equivalent in the trimer (i.e., $S_{trimer} = S_1 + S_2 + S_3 \neq 0$), and the ground state of the total spin of the M_3O_{12} trimer should strongly contribute to the magnetic properties of $Ba_4LnM_3O_{12}$. Previously, we prepared a series of quadruple perovskites $Ba_4LnM_3O_{12}$ (Ln = rare earths; M = Ru, Ir), and determined their crystal structures from powder X-ray and neutron diffraction measurements. Through magnetic susceptibility measurements, magnetic properties of each compound were determined [57-60].

In order to elucidate the role of the trimer M_3O_{12} in the magnetic behavior of $Ba_4LnM_3O_{12}$, we re-measured magnetic susceptibilities and specific heat for some of the $Ba_4LnM_3O_{12}$, and performed electrical resistivity measurements. Magnetic properties of quadruple perovskites $Ba_4LnM_3O_{12}$ were also compared with those of triple perovskites $Ba_3LnM_2O_9$ and double perovskites Ba_2LnMO_6 to understand how the difference in the connection of the BO_6 octahedra (i.e., face-sharing and corner-sharing) affects the magnetic properties of the perovskites.

2. Experimental

2.1. Preparation

Polycrystalline samples of $Ba_4LnRu_3O_{12}$ (Ln = La–Nd, Sm–Lu) were prepared by the standard solid-state reaction. BaO, BaO_2, Ru, RuO_2, and Ln_2O_3 were used as starting materials. They were well mixed in an agate mortar. The mixtures were pressed into pellets and enclosed

with platinum tubes, and they were sealed in evacuated silica tubes. They were fired at 1250°C for 12–204 h. Details were described elsewhere [57, 58, 60].

2.2. X-ray diffraction analysis

The obtained phases were identified by powder X-ray diffraction (XRD) measurements. They were performed with using a Rigaku Multi-Flex diffractometer with Cu-Kα radiation. The data were collected by step-scanning in the angle range of $10° \leq 2\theta \leq 120°$ at a 2θ step-size of 0.02°. The X-ray diffraction data were analyzed by the Rietveld technique, using the programs RIETAN2000 [61].

2.3. Magnetic susceptibility measurements

The temperature-dependence of the magnetic susceptibility was measured in an applied field of 0.1 T over the temperature range of 1.8 K $\leq T \leq$ 400 K, using a SQUID magnetometer (Quantum Design, MPMS5S).

2.4. Specific heat measurements

Specific heat measurements were performed using a relaxation technique by a commercial heat capacity measuring system (Quantum Design, PPMS) in the temperature range of 0.5-400 K. The sintered sample in the form of a pellet was mounted on a thin alumina plate with Apiezon grease for better thermal contact.

2.5. Electrical resistivity measurements

The temperature dependence of the electrical resistivity was measured by the dc four-probe technique in the temperature range of 60-1,000 K. The sample was sintered and then cut into a piece approximately 3.5 mm $\times$ 3.5 mm $\times$ 1 mm in size.

3. Results and Discussion

3.1. Structures and the oxidation states of $Ba_4LnM_3O_{12}$

Quadruple perovskites $Ba_4LnM_3O_{12}$ (Ln = La-Nd, Sm-Lu; M = Ru, Ir) were prepared as a single phase. The powder X-ray diffraction measurements and their Rietveld analysis show that the $Ba_4LnRu_3O_{12}$ for Ln = Tb-Lu have a hexagonal unit cell with space group R-$3m$ (No.166) (Fig. 1 (d)), while those for Ln = La-Nd, Sm-Gd have a monoclinic unit cell with space group $C2/m$ (No.12) due to the larger difference in the ionic radius between Ln and Ru [57]. On the other hand, all the iridium compounds $Ba_4LnIr_3O_{12}$ were indexed with the monoclinic unit cell. Structural parameters were summarized in Supplementary tables 1-3. Figure 2 shows the monoclinic perovskite structure with 12 layers for $Ba_4LnM_3O_{12}$ (Ln = La-Gd for M = Ru; Ln =La~Lu for M = Ir). In this structure, M ions are octahedrally coordinated by six oxide ions, and three MO_6 octahedra share faces forming a M_3O_{12} trimer. The M_3O_{12} trimers and LnO_6 octahedra are alternately linked by corner-sharing and form the perovskite-type structure with 12 layers. The M-M interatomic distances in the M_3O_{12} trimer are 2.4~2.6 Å for both $Ba_4LnRu_3O_{12}$ and $Ba_4LnIr_3O_{12}$ compounds. These distances are much shorter than double the metallic radius of Ru and Ir (2.72 Å) [62], indicating that strong interactions between M ions should exist in the M_3O_{12} trimer.

The lattice parameters and volumes of $Ba_4LnM_3O_{12}$ were plotted against the ionic radius of Ln^{3+} in Fig. 3. Except for the compounds having Ln = Ce, Pr, and Tb, the lattice parameters a, b, c, and β monotonously increase with the Ln^{3+} ionic radius. However, the values for Ln = Ce, Pr, and Tb compounds are considerably smaller than this trend. Table 1 lists the refined Ln-O bond lengths for Ln = Ce, Pr, and Tb compounds. For both M = Ru and Ir cases, these bond lengths are close to the Ln^{4+}-O^{2-} lengths calculated from Shannon's ionic radii [63]. These results show that the Ce, Pr, and Tb ions are in the tetravalent state. Therefore, the oxidation states of Ru and Ir are also tetravalent ($Ba_4Ln^{4+}Ru^{4+}_3O_{12}$, $Ba_4Ln^{4+}Ir^{4+}_3O_{12}$). For other Ln ions, the mean oxidation state of Ru and Ir ions is +4.33 ($Ba_4Ln^{3+}Ru^{4.33+}_3O_{12}$, $Ba_4Ln^{3+}Ir^{4.33+}_3O_{12}$).

3.2. Magnetic properties of $Ba_4Ln^{3+}M^{4.33+}_3O_{12}$

Measurements of the magnetic susceptibility for $Ba_4LnM_3O_{12}$ give the contrastive results between the ruthenium-containing compounds $Ba_4LnRu_3O_{12}$ and the iridium-containing compounds $Ba_4LnIr_3O_{12}$, and the results are summarized in Table 2. Any of the $Ba_4Ln^{3+}Ru^{4.33+}_3O_{12}$ compounds shows similar magnetic transitions at very low temperatures, whereas $Ba_4Ln^{3+}Ir^{4.33+}_3O_{12}$ ($Ln \neq$ La, Lu) compounds are paramagnetic down to 1.8 K.

Magnetic properties of $Ba_4Ln^{3+}Ir^{4.33+}_3O_{12}$ clearly show that we have to treat the M ions as the M_3O_{12} trimer to understand their magnetic behavior. Both compounds $Ba_4Ln^{3+}Ir^{4.33+}_3O_{12}$ (Ln = La, Lu) are diamagnetic, indicating that the $Ir^{4.33+}_3O_{12}$ trimers are diamagnetic. Other compounds $Ba_4Ln^{3+}Ir^{4.33+}_3O_{12}$ (i.e., $Ln \neq$ La, Lu) are paramagnetic down to 1.8 K, and their effective magnetic moments (μ_{eff}) are close to the magnetic moments of Ln^{3+} ions (μ_{Ln}) (see Table 3). That is, the contribution of the $Ir^{4.33+}_3O_{12}$ trimer to the magnetic properties of $Ba_4LnIr_3O_{12}$ is negligible.

As described above section, the distances between Ir atoms in the Ir_3O_{12} trimer are 2.48~2.60 Å. The short Ir-Ir interatomic distances in the Ir_3O_{12} trimer suggest the overlap of metal d orbitals having lobes along the threefold symmetry axis, which means the formation of molecular orbitals in the Ir_3O_{12} trimer. The electronic structure of Ru_3Cl_{12} with D_{3h} point symmetry has been described [64]. The energy level scheme of Ir_3O_{12} in the $Ba_4LnIr_3O_{12}$ should be similar to the case of Ru_3Cl_{12}, but the degenerated energy levels are expected to be split into more levels due to the monoclinic distortion of the Ir_3O_{12} trimer and to the spin-orbit coupling of the $5d$ electrons (Ir ions). The electronic configuration of the $Ir^{4.33+}_3O_{12}$ trimer (the number of $5d$ electrons is 14) with D_{3h} point symmetry is $(a_{1g})^2(e_g)^4(a_{2u})^2(e_u)^4(e_g)^2$, and the schematic energy level diagrams for the Ir-Ir interactions in the $Ir^{4.33+}_3O_{12}$ trimer are illustrated in Fig. 4 (c). The highest occupied e_g orbital of the Ir_3O_{12} trimer should be split into two singlets by the monoclinic distortion, which causes the $S = 0$ ground state of the filled HOMO level ($S_{\text{trimer}} = 0$). Therefore, the $Ir^{4.33+}_3O_{12}$ trimer does not contribute to the magnetic properties of $Ba_4LnIr_3O_{12}$

(Ln = La, Nd-Gd, Dy-Lu), and both $Ba_4LaIr_3O_{12}$ and $Ba_4LuIr_3O_{12}$ are diamagnetic.

In a similar way as the case for the Ir_3O_{12} trimer, the electronic configuration of the $Ru^{4.33+}_3O_{12}$ trimer (the number of $4d$ electrons is 11) with D_{3h} point symmetry is $(a_{1g})^2(e_g)^4(a_{2u})^2(e_u)^3$ and the schematic energy level diagrams are illustrated in Fig. 4 (a). The highest occupied e_u orbital has the S = 1/2 ground state. Therefore, the $Ru^{4.33+}_3O_{12}$ trimer (S_{trimer} = 1/2) contributes to the magnetic properties of $Ba_4LnRu_3O_{12}$. Figure 5 shows the temperature dependence of the magnetic susceptibility for $Ba_4LaRu_3O_{12}$. Both $Ba_4LaRu_3O_{12}$ and $Ba_4LuRu_3O_{12}$ order antiferromagnetically at 6.0, and 8.0 K, respectively. Since La^{3+} and Lu^{3+} ions are diamagnetic, the $Ru^{4.33+}_3O_{12}$ trimers are antiferromagnetically coupled. Other $Ba_4LnRu_3O_{12}$ compounds show similar antiferromagnetic transitions at comparable temperatures, which should be due to the magnetic ordering of the $Ru^{4.33+}_3O_{12}$ trimers.

3.3. Magnetic properties of $Ba_4Ln^{4+}M^{4+}_3O_{12}$

Figure 6 shows the temperature dependences of the magnetic susceptibility for $Ba_4CeM_3O_{12}$ (M = Ru, Ir). Since the tetravalent Ce^{4+} ion is diamagnetic, only the M^{4+} ions (*i.e.*, Ru^{4+} and Ir^{4+} ions) contribute to the magnetic properties of $Ba_4CeM_3O_{12}$ compounds. Magnetic behavior at low temperatures is different between these two compounds, i.e., the iridium-containing compound $Ba_4CeIr_3O_{12}$ antiferromagnetically orders at 10.5 K, while the ruthenium-containing compound $Ba_4CeRu_3O_{12}$ shows no magnetic ordering down to 0.5 K. This magnetic behavior of $Ba_4Ln^{4+}M^{4+}_3O_{12}$ is understandable by considering the magnetic properties of $M^{4+}_3O_{12}$ trimer.

In the same way as the case of $Ir^{4.33+}_3O_{12}$, the $Ir^{4+}_3O_{12}$ trimer has fifteen $5d$ electrons, and its electronic configuration is $(a_{1g})^2(e_g)^4(a_{2u})^2(e_u)^4(e_g)^3$. The highest occupied e_g orbitals (doublet) have the S = 1/2 ground state (see Fig. 4 (d)). The antiferromagnetic ordering of $Ba_4CeIr_3O_{12}$ is due to this ground S = 1/2 state. On the other hand, the electronic configuration of the $Ru^{4+}_3O_{12}$ trimer is $(a_{1g})^2(e_g)^4(a_{2u})^2(e_u)^4$, indicating the S = 0 state of the filled HOMO, as shown in Fig. 4 (b). Therefore, $Ba_4CeRu_3O_{12}$ should be diamagnetic and shows no magnetic ordering. Actually

8

it is weakly paramagnetic, indicating that the molecular orbital model is not perfect for the case of Ru_3O_{12} trimer. We have to consider the excited state. This is because the $4d$ electrons are somewhat more localized than the $5d$ electrons.

The magnetic susceptibility vs. temperature curves for $Ba_4PrM_3O_{12}$ (M = Ru, Ir) are depicted in Fig. 7, indicating an antiferromagnetic transition at 2.4 K (M = Ru) and 35 (M = Ir). Since $Ba_4CeRu_3O_{12}$ shows no long-range magnetic ordering down to 0.5 K, the magnetic anomaly observed at 2.4 K in $Ba_4PrRu_3O_{12}$ is due to the magnetic interactions of the magnetic moment of Pr^{4+} ions. The results of the specific heat measurements have cleared this point.

3.4. Specific heat of Ba$_4$LnM$_3$O$_{12}$ (Ln = Ce, Pr; M = Ru, Ir)

Figure 8 (a) shows the temperature dependence of the specific heat (C_p) for $Ba_4PrRu_3O_{12}$ together with that for $Ba_4CeRu_3O_{12}$. A specific heat anomaly has been observed at 2.4 K, indicating that the long-range antiferromagnetic ordering occur at this temperature. In order to evaluate the magnetic entropy change due to the observed transition for $Ba_4PrRu_3O_{12}$, following procedures were performed. Magnetic contribution to the specific heat (C_{mag}) of $Ba_4PrRu_3O_{12}$ was evaluated by subtracting the contribution of the lattice specific heat (C_{lat}) from the total specific heat ($C_{mag} = C_p - C_{lat}$). The lattice specific heat (C_{lat}) from the total specific heat was estimated by using the specific heat data of $Ba_4CeRu_3O_{12}$. By the relation $S_{mag} = \int (C_{mag}/T) dT$, the magnetic entropy change for $Ba_4PrRu_3O_{12}$ was calculated to be 5.20 J/mol K, which is near to $R \ln2 = 5.76$ J/mol K (R : gas constant) (Fig. 8 (b)). This result clearly shows that the antiferromagnetic ordering is due to the ground Kramers doublet of Pr^{4+} in a low-symmetric crystal field.

Figure 8 (c) shows the temperature dependence of the specific heat divided by temperature (C_p/T) for the iridium-containing two compounds $Ba_4LnIr_3O_{12}$ (Ln = Ce, Pr). The magnetic ordering temperature for $Ba_4PrIr_3O_{12}$ (35 K) is much higher than that for $Ba_4CeIr_3O_{12}$ (10.5 K). This result indicates that not only the Ir_3O_{12} trimer but also the Pr^{4+} ion contribute to the

antiferromagnetic interaction of the $Ba_4PrIr_3O_{12}$. The magnetic entropy change of $Ba_4PrIr_3O_{12}$ is obtained to be 8.7 J/mol K. Since the corresponding ruthenium-containing compound $Ba_4PrRu_3O_{12}$ shows an antiferromagnetic transition at 2.4 K, and since its transition is due to the ground Kramers doublet of Pr^{4+} ion from the specific heat measurements, the contribution of the $Ir^{4+}_3O_{12}$ trimer to the antiferromagnetic transition of $Ba_4PrIr_3O_{12}$ is estimated to be R ln2. That is, the magnetic behavior of $Ir^{4+}_3O_{12}$ trimer is the one with $S = 1/2$, which is consistent with the above-mentioned discussion using the molecular orbital diagram for the M_3O_{12} trimer (Fig. 4 (d)).

3.5. Effective magnetic moments of $Ba_4LnM_3O_{12}$ (Ln = La ~ Lu; M = Ru, Ir)

As described already, the effective magnetic moments of $Ba_4Ln^{3+}Ir^{4.33+}_3O_{12}$ compounds (μ_{eff}) are close to the magnetic moments of Ln^{3+} ions (μ_{Ln}) (Table 3). That is, since the $Ir^{4.33+}_3O_{12}$ trimer has the $S = 0$ ground state, its contribution to the magnetic properties of $Ba_4Ln^{3+}Ir^{4.33+}_3O_{12}$ is negligible. For the case of $Ba_4Ln^{4+}Ir^{4+}_3O_{12}$ (Ln = Ce, Pr, Tb) compounds, the ground state of the $Ir^{4+}_3O_{12}$ trimer is $S = 1/2$. Therefore, the effective magnetic moments should be calculated from the equation $\mu_{cal} = \sqrt{\mu_{Ln^{4+}}^2 + \mu_{S=1/2}^2}$, and they are also listed in Table 3. The effective magnetic moments of $Ba_4Ln^{4+}Ir^{4+}_3O_{12}$ are almost in accordance with the calculated moments.

In the same way as the case of $Ba_4Ln^{4+}Ir^{4+}_3O_{12}$, both the Ln^{3+} ion and $Ru^{4.33+}_3O_{12}$ trimer contribute to the magnetic properties of the $Ba_4Ln^{3+}Ru^{4.33+}_3O_{12}$, because the $Ru^{4.33+}_3O_{12}$ trimer has the $S = 1/2$ ground state. The effective magnetic moments of the $Ba_4Ln^{3+}Ru^{4.33+}_3O_{12}$ compounds should be calculated from the equation,

$$\mu_{cal} = \sqrt{\mu_{Ln^{3+}}^2 + \mu_{S=1/2}^2} , \qquad (1)$$

and they are shown in Fig. 9. Experimental values are comparable with the calculated moments (Eq.(1)) and are much smaller than the moments calculated from the contribution of each ion ($Ln^{3+} + 2Ru^{4+} + Ru^{5+}$),

$$\mu_{cal} = \sqrt{\mu_{Ln^{3+}}^2 + 2\mu_{Ru^{4+}}^2 + \mu_{Ru^{5+}}^2}.$$ (2)

3.6. Magnetic transition temperatures of $Ba_{n+1}LnRu_nO_{3n+3}$ (n = 1, 2, 3)

Figure 10 shows the magnetic transition temperatures of $Ba_4LnRu_3O_{12}$ with those of $Ba_3LnRu_2O_9$ and Ba_2LnRuO_6. It is clear that magnetic transition temperatures of the double perovskites Ba_2LnRuO_6 (n = 1) are considerably higher than those of $Ba_3LnRu_3O_9$ (n = 2) and $Ba_4LnRu_3O_{12}$ (n = 3). This is due to the fact that the magnetic interaction of Ba_2LnRuO_6 is via the almost linear pathway of Ln-O-Ru [22]. Therefore, the Ln ions greatly contribute to the antiferromagnetic ordering of Ba_2LnRuO_6, and their transition temperatures are considerably different among Ba_2LnRuO_6 compounds.

The situation for the quadruple perovskites $Ba_4LnRu_3O_{12}$ is quite different from that for Ba_2LnRuO_6. Any of the $Ba_4Ln^{3+}Ru^{4.33+}_3O_{12}$ compounds shows magnetic anomaly at lower temperatures, and their transition temperatures are comparable among $Ba_4LnRu_3O_{12}$ compounds. On the other hand, the iridium-containing compounds $Ba_4Ln^{3+}Ir^{4.33+}_3O_{12}$ are paramagnetic down to 1.8 K, and their magnetic properties are due to the magnetic behavior of Ln^{3+} ions (Table 3) (because the ground state of the $Ir^{4.33+}_3O_{12}$ trimer is $S_{trimer} = 0$). These results indicate that the antiferromagnetic transition observed in the $Ba_4Ln^{3+}Ru^{4.33+}_3O_{12}$ is mainly due to the magnetic behavior of the $Ru^{4.33+}_3O_{12}$ trimer with $S = 1/2$. The results on magnetic susceptibility and specific heat measurements for $Ba_3Ln^{3+}Ru^{4.5+}_2O_9$ compounds also show that the antiferromagnetic interaction is ascribed to the behavior of $Ru^{4.5+}_2O_9$ dimer ($S = 1/2$) [46, 48].

All the $Ba_4Ln^{4+}Ir^{4+}_3O_{12}$ compounds (Ln = Ce, Pr, Tb) show an antiferromagnetic transition at lower temperatures (Table 2), and it has been found that the $Ir^{4+}_3O_{12}$ trimer with $S = 1/2$ contributes to the magnetic transition from the specific heat measurements. The corresponding $Ba_4Ce^{4+}Ru^{4+}_3O_{12}$ compound does not show any magnetic ordering (because the Ce^{4+} ion is diamagnetic and the $Ru^{4+}_3O_{12}$ trimer has the $S = 0$ ground state). Both $Ba_4Pr^{4+}Ru^{4+}_3O_{12}$ and $Ba_4Tb^{4+}Ru^{4+}_3O_{12}$ compounds show an antiferromagnetic transition at 2.4 and 24 K, which are

11

due to the antiferromagnetic ordering of the magnetic moments of Pr^{4+} (Tb^{4+}) ions from the specific heat and neutron diffraction measurements [57].

3.7. Electrical resistivity of Ba$_4$LnM$_3$O$_{12}$

The electrical resistivity of $Ba_4EuM_3O_{12}$ (M = Ru, Ir) is plotted as a function of reciprocal temperature in Fig. 11 (a). All the $Ba_4LnM_3O_{12}$ compounds are nonmetallic in the temperature range $60 < T < 1{,}000$ K, showing the increasing resistance with decreasing temperature. Attempts to fit the observed data to a simple Arrhenius model were unsuccessful. The Mott variable-range hopping (VRH) model [65],

$$\rho \propto \exp\left\{(T_0/T)^{1/(n+1)}\right\},\qquad(3)$$

was taken into account. When the parameter n is 2, experimental data show good linearity (see Fig. 11 (b)), suggesting that the semiconducting behavior of $Ba_4LnM_3O_{12}$ may be attributable to the variable-range hopping in two-dimensions. The crystal structure of $Ba_4LnM_3O_{12}$ can be expressed by the alternate stacking of two kinds of two-dimensional layers which consisit of the LnO_6 octahedra or the M_3O_{12} trimers. This structural feature may account for the observed resistivity behavior.

4. Conclusions

Quadruple perovskites $Ba_4LnM_3O_{12}$ (Ln = rare earths; M = Ru, Ir) crystallize in the 12L-perovskite-type structure. Three MO_6 octahedra are connected to each other by face-sharing and form a M_3O_{12} trimer. The M_3O_{12} trimers and LnO_6 octahedra are alternately linked by corner-sharing, forming the perovskite-type structure with 12 layers. All the $Ba_4Ln^{3+}Ru^{4.33+}_3O_{12}$ compounds show magnetic ordering at low temperatures, while any of the corresponding iridium-containing compounds $Ba_4Ln^{3+}Ir^{4.33+}_3O_{12}$ is paramagnetic down to 1.8 K. $Ba_4Ce^{4+}Ir^{4+}_3O_{12}$ orders antiferromagnetically at 10.5 K, while the corresponding ruthenium-containing compound $Ba_4Ce^{4+}Ru^{4+}_3O_{12}$ is paramagnetic. These magnetic results were well understood by considering the magnetic behavior of the M_3O_{12} trimer.

References

[1] J. M. Longo and J. A. Kafalas, *J. Solid State Chem.*, **1** (1969) 103−108.

[2] P.D. Battle, J.B. Goodenough, and R. Price, *J. Solid State Chem.*, **46** (1983) 234-244.

[3] P.D. Battle and W.J. Macklin, *J. Solid State Chem.*, **52** (1984) 138-145.

[4] P.D. Battle and W.J. Macklin, *J. Solid State Chem.*, **54** (1984) 245-250.

[5] P.D. Battle and C.W. Jones, *J. Solid State Chem.*, **78** (1989) 108-116.

[6] P.D. Battle, C.W. Jones, and F. Studer, *J. Solid State Chem.*, **90** (1991) 302-312.

[7] M. T. Anderson, K. B. Greenwood, G. A. Taylor, and K. R. Poeppelmeier, *Proc. Solid State Chem.*, **22** (1993) 197-233.

[8] D. Harada, M. Wakeshima and Y. Hinatsu, *J. Solid State Chem.*, **145** (1999) 356-360.

[9] Y. Doi and Y. Hinatsu, *J. Phys.: Condens. Matter*, **11** (1999) 4813-4820.

[10] M. Wakeshima, D. Harada, and Y. Hinatsu, *J. Alloys and Compd.*, **287** (1999) 130-136.

[11]D. Harada, M. Wakeshima, Y. Hinatsu, K.Ohoyama, and Y.Yamaguchi, *J. Phys.: Condens. Matter*, **12** (2000) 3229-3239.

[12] M. Wakeshima, D. Harada, and Y. Hinatsu, *J. Mater. Chem.*, **10** (2000) 419-422.

[13] Y. Doi, Y. Hinatsu, K. Oikawa, Y. Shimojo, and Y. Morii, *J. Mater. Chem.*, **10** (2000) 797-800.

[14] Y. Izumiyama, Y. Doi, M. Wakeshima, Y. Hinatsu, K. Oikawa, Y. Shimojo, and Y. Morii, *J. Mater. Chem.*, **10** (2000) 2364-2367.

[15] Y. Izumiyama, Y. Doi, M. Wakeshima, Y. Hinatsu, Y. Shimojo, and Y. Morii, *J. Phys.: Condens. Matter*, **13** (2001) 1303-1313.

[16] M. Wakeshima, Y. Izumiyama, Y. Doi, and Y. Hinatsu, *Solid State Commun.*, **120** (2001) 273-278.

[17] Y. Izumiyama, Y. Doi, M. Wakeshima, Y. Hinatsu, A. Nakamura, and Y. Ishii, *J. Solid State Chem.*, **169** (2002) 125-130.

[18] Y. Hinatsu and Y. Doi, *Bull. Chem. Soc. Japan*, **76** (2003) 1093-1113.

[19] N. G. Parkinson, P. D. Hatton, J. A. K. Howard, C. Ritter, R. M. Ibberson, and M-K Wu, *J. Phys.: Condens. Matter*, **16** (2004) 7611-7624.

[20] L. Li and B. J. Kennedy, *J. Solid State Chem.*, **177** (2004) 3290-3300.

[21] B. J. Kennedy, L. Li, Y. Lee, T. Vogt, and B. J. Kennedy, *J. Phys.: Condens. Matter*, **16** (2004) 3295-3301.

[22] C. Sakai, Y. Doi, Y. Hinatsu, and K. Ohoyama, *J. Phys.: Condens. Matter*, **17** (2005) 7383-7394.

[23] Q. Zhou, B. J. Kennedy, K.S. Wallwork, M. Elcombe, Y. Lee, and T. Vogt, *J. Solid State Chem.*, **178** (2005) 2282-2291.

[24] C. Sakai, Y. Doi, and Y. Hinatsu, *J. Alloys and Compd*, **408-412** (2006) 608-612.

[25] W. Kockelmann, D. T. Adroja, A D. Hillier, M. Wakeshima, Y. Izumiyama, Y. Hinatsu, K. S. Knight, D. Visser, and B. D. Rainford, *Physica B,* **378-380** (2006) 543-545.

[26] R. Saez-Puche, E. Climent-Pascual, R. Ruiz-Bustos, M. A. Alario-Franco, and M. T. Fernandez-Diaz, *Progress in Solid State Chem.*, **35** (2007) 211-219.

[27] R. C. Bryne and C. W. Moeller, *J. Solid State Chem.*, **2** (1970) 228−235.

[28] J. Darriet, M. Drillon, G. Villeneuve, and P. Hagenmuller, *J. Solid State Chem.*, **19** (1976) 213−220.

[29] H.-U. Schaller and S. Kemmler-Sack, *Z. Anorg. Allg. Chem.*, **473** (1981) 178-188.

[30] I. Thumm, U. Treiber, and S. Kemmler-Sack, *Z. Anorg. Allg. Chem.*, **477** (1981) 161-166.

[31] U. Treiber, S. Kemmler-Sack, A. Ehmann, H.-U. Schaller, E. Dürrschmidt, I. Thumm and H. Bader, *Z. Anorg. Allg. Chem.*, **481** (1981) 143-152.

[32] H. W. Zandbergen and D. J. W. IJdo, *Acta Crystallogr.*, C**40** (1984) 919-922.

[33] D. Verdoes, H. W. Zandbergen, and D. J. W. IJdo, *Acta Crystallogr.*, C**41** (1985) 170-173.

[34] P. Lightfoot and P. D. Battle, *J. Solid State Chem.*, **89** (1990) 174−183.

[35] P.D. Battle, S. H. Kim, and A. V. Powell, *J. Solid State Chem.*, **101** (1992) 161-172.

[36] D. Schluter and H.-K. Müller-Buschbaum, *J. Alloys and Compd.*, **190** (1993) L43-L44.

[37] S. Scheske and H.-K. Müller-Buschbaum, *J. Alloys and Compd.*, **198** (1993) 173-176.

[38] M. Rath and H.-K. Müller-Buschbaum, *J. Alloys and Compd.*, **210** (1994) 119-123.

[39] S. H. Kim and P.D. Battle, *J. Solid State Chem.*, **114** (1995) 174-183.

[40] P.D. Battle, J. G. Gore, R. C. Hollyman, and A. V. Powell, *J. Alloys and Compd*, **218** (1995) 110-116.

[41] D.-K. Jung, G. Demazeau, J. Etourneau, and M. A. Subramanian, *Mater. Res. Bull.*, **30** (1995) 113-123.

[42] J. T. Rijssenbeek, P. Matl, B. Batlogg, N. P. Ong, and R. J. Cava, *Phys.Rev.*, **58** (1998) 10315−10318.

[43] J. T. Rijssenbeek, Q. Huang, R. W. Erwin, H. W. Zandbergen, and R. J. Cava, *J. Solid State Chem.*, **146** (1999) 65−72.

[44] Y. Doi, Y. Hinatsu, Y. Shimojo, and Y. Ishii, *J. Solid State Chem.*, **161** (2001) 113-120.

[45] Y. Doi, M. Wakeshima, Y. Hinatsu, A. Tobo, K. Ohoyama, and Y. Yamaguchi, *J. Mater. Chem.*, **11** (2001) 3135–3140.

[46] Y. Doi, K. Matsuhira, and Y. Hinatsu, *J. Solid State Chem.*, **165** (2002) 317-323.

[47] K. E. Stitzer, M. D. Smith, W. R. Gemmill, and H.-C. zur Loye, *J. Am. Chem. Soc.*, **124** (2002) 13877–13885.

[48] Y. Doi and Y. Hinatsu, *J. Mater. Chem.*, **12** (2002) 1792-1795.

[49] E. Quarez, M. Huve, F. Abraham, and O. Mentre, *Solid State Sci.*, **5** (2003) 951-963.

[50] Y. Doi and Y. Hinatsu, *J. Phys.: Condens. Matter*, **16** (2004) 2849–2860.

[51] Y. Doi and Y. Hinatsu, *J. Solid State Chem.*, **177** (2004) 3239-3244.

[52] M. W. Lufaso and H.-C. zur Loye, *Inorg. Chem.*, **44** (2005) 9143–9153.

[53] M. W. Lufaso and H.-C. zur Loye, *Inorg. Chem.*, **44** (2005) 9154–9161.

[54] C. H. De Vreugd, H. W. Zandbergen, and D. J. W. IJdo, *Acta Crystallogr.*, C**40** (1984) 1987-1989.

[55] A. F. Fuentes, K. Boulahya, and U. Amador, *J. Solid State Chem.*, **177** (2004) 714-720.

[56] N. Creon, C. Michel, M. Hervieu, A. Maignan, and B. Raveau, *Solid State Sci.*, **5** (2003) 243-248.

[57] Y. Shimoda, Y. Doi, Y. Hinatsu, and K. Ohoyama, *Chem. Mater.*, **20** (2008) 4512-4518.

[58] Y. Shimoda, Y. Doi, M. Wakeshima, and Y. Hinatsu, *J. Solid State Chem.*, **182** (2009) 2873-2879.

[59] Y. Shimoda, Y. Doi, M. Wakeshima, and Y. Hinatsu, *Inorg. Chem.*, **48** (2009) 2104-2110.

[60] Y. Shimoda, Y. Doi, M. Wakeshima, and Y. Hinatsu, *J. Solid State Chem.*, **183** (2010) 33-40.

[61] F. Izumi and T. Ikeda, *Mater. Sci. Forum*, **321–324** (2000) 198–203.

[62] A. F. Wells, *Structural inorganic chemistry 5ᵗʰ Ed.*, Oxford Clarendon Press (1984).

[63] R. D. Shannon, *Acta Crystallogr.*, Sect. A, **32** (1976) 751-767.

[64] B. E. Bursten, F. A. Cotton, and A. Fang, *Inorg. Chem.*, **22** (1983) 2127-2133.

[65] N. F. Mott and E. A. Davis, "Electronic Processes in Non-Crystalline Materials," 2nd ed, Clarendon Press, Oxford (1979).

Fig. 1   Schematic crystal structures of (a) cubic double perovskite Ba_2LnMO_6, (b) the stacking

sequence of the double perovskite (*abc…*), (c) hexagonal triple perovskite $Ba_3LnM_2O_9$

(the stacking sequence: *abacbc*...), and (d) hexagonal quadruple perovskite

$Ba_4LnM_3O_{12}$ (the stacking sequence: *ababcacabcbc*...).

Fig. 2   The monoclinic perovskite structure with 12 layers for $Ba_4LnM_3O_{12}$ (Ln = La-Gd for

M = Ru; Ln =La~Lu for M = Ir)

Fig. 3   Variation of lattice parameters and volumes for $Ba_4LnM_3O_{12}$ against the ionic radius of

Ln^{3+} (M = Ru, circles; M = Ir, squares). (a) a (●, ■) : for monoclinic structures,

values of $a/\sqrt{3}$ are plotted; b(○, □), (b) c, (c) β, and (d) volume V: for monoclinic

structures, half of the volumes are plotted.

Fig. 4   Schematic energy level diagrams for (a) $Ru^{4.33+}_3O_{12}$ trimer, (b) $Ru^{4+}_3O_{12}$ trimer, (c)

$Ir^{4.33+}_3O_{12}$ trimer, and (d) $Ir^{4+}_3O_{12}$ trimer.

Fig. 5   Temperature dependence of the magnetic susceptibility for $Ba_4LaRu_3O_{12}$. The inset

shows the reciprocal susceptibility against temperature.

Fig. 6   Temperature dependence of the magnetic susceptibilities for $Ba_4CeM_3O_{12}$ (M = Ru, Ir).

The inset shows the magnetic susceptibilities of $Ba_4CeIr_3O_{12}$ at low temperatures.

Fig. 7   Temperature dependence of the magnetic susceptibilities for $Ba_4PrM_3O_{12}$ (M = Ru, Ir).

The inset shows the magnetic susceptibilities of $Ba_4PrRu_3O_{12}$ at low temperatures.

Fig. 8   (a) Temperature dependence of the specific heat (C_p) for $Ba_4LnRu_3O_{12}$ (Ln = Ce, Pr).

(b) The magnetic specific heat divided by temperature (C_{mag}/T) and the magnetic

entropy (S_m) of $Ba_4PrRu_3O_{12}$. (c) Temperature dependence of the specific heat divided

by temperature (C_p/T) for $Ba_4LnIr_3O_{12}$ (Ln = Ce, Pr).

Fig. 9   Comparison of the effective magnetic moments of $Ba_4Ln^{3+}Ru^{4.33+}_3O_{12}$ with the

calculated values.

Fig.10   Magnetic transition temperatures of $Ba_{n+1}Ln Ru_nO_{3n+3}$.

Fig.11   Temperature dependence of the resistivity for $Ba_4EuM_3O_{12}$ (M = Ru, Ir).

(a) log ρ vs T^{-1} plot; (b) log ρ vs $T^{-1/3}$ plot.

Table 1   Average Ln–O bond lengths $d(Ln$–O) determined for $Ba_4LnM_3O_{12}$ (Ln = Ce, Pr, Tb; M = Ru, Ir) and bond lengths (d_{cal}) calculated from Shannon's ionic radii [Ref.63].

| | $d(Ln$–O$)$ / Å | | d_{cal} / Å | |
Ln	$Ba_4LnRu_3O_{12}$	$Ba_4LnIr_3O_{12}$	Ln^{3+}–O^{2-}	Ln^{4+}–O^{2-}
Ce	2.21	2.19	2.41	2.27
Pr	2.18	2.24	2.39	2.25
Tb	2.08	2.17	2.32	2.16

Table 2　Magnetic properties of $Ba_4LnM_3O_{12}$ (Ln = Rare Earths; M = Ru, Ir).

Ln	Valence state of Ln ion	Magnetic properties $Ba_4LnRu_3O_{12}$	(Transition temperature / K) $Ba_4LnIr_3O_{12}$
La	3+	AF(6.0)	Dia
Ce	**4+**	CW	AF (10.5)
Pr	**4+**	AF (2.4)	AF (35)
Nd	3+	F (11)	CW
Sm	3+	AF (3.2)	van Vleck
Eu	3+	AF (4.0)	van Vleck
Gd	3+	AF (2.5)	CW
Tb	**4+**	AF (24)	AF (16)
Dy	3+	AF (30)	CW
Ho	3+	AF (8.5)	CW
Er	3+	AF (8.0)	CW
Tm	3+	AF (8.0)	CW
Yb	3+	AF (4.8)	CW
Lu	3+	AF (8.0)	Dia

Note: AF: antiferromagnetic, F: ferrimagnetic, CW: Curie-Weiss, Dia: diamagnetic.

Table 1 Effective magnetic moments of $Ba_4LnIr_3O_{12}$

$Ba_4Ln^{3+}Ir^{4.33+}_3O_{12}$	Electronic configuration	J	μ_{eff}/μ_B	$\mu_{Ln}{}^a/\mu_B$
La^{3+}	$4f^0$	0	—	—
Nd^{3+}	$4f^3$	9/2	3.60	3.62
Sm^{3+}	$4f^5$	5/2		0.84
Eu^{3+}	$4f^6$	0	—	—
Gd^{3+}	$4f^7$	7/2	7.98	7.94
Dy^{3+}	$4f^9$	15/2	10.71	10.63
Ho^{3+}	$4f^{10}$	8	10.36	10.60
Er^{3+}	$4f^{11}$	15/2	9.21	9.59
Tm^{3+}	$4f^{12}$	6	7.31	7.57
Yb^{3+}	$4f^{13}$	7/2	3.86	4.54
Lu^{3+}	$4f^{14}$	0	—	—

$Ba_4Ln^{4+}Ir^{4+}_3O_{12}$	Electronic configuration	J	μ_{eff}/μ_B	$\mu_{cal}{}^b/\mu_B$
Ce^{4+}	$4f^0$	0	1.61	1.73
Pr^{4+}	$4f^1$	5/2	2.94	3.07
Tb^{4+}	$4f^7$	7/2	8.02	8.13

[a] μ_{Ln}: free ion values of Ln^{3+}.

[b] $\mu_{cal} = \sqrt{\mu_{Ln^{4+}}{}^2 + \mu_{S=1/2}{}^2}$.

(a)

LnO$_6$ Ba

MO$_6$

(b)

3-layers

a
c
b
a

(c)   6-layers

a
c
b
c
a
b
a

(d)   12-layers

a
c
b
c
b
a
c
a
c
b
a
b
a

Fig.1

LnO$_6$ octahedron

Ba

M$_3$O$_{12}$ trimer

c

a

b

Fig. 2

Fig. 3

(a)   (b)   (c)   (d)

a_{1g}

e_g

$D_{3h} \rightarrow C_2$

$d\delta$
$d\sigma$

outer M ions

e_u
a_{2u}

e_g

a_{1g}

$d\delta$
$d\sigma$

inner M ion

$Ru^{4.33+}_3O_{12}$ $Ru^{4+}_3O_{12}$ $Ir^{4.33+}_3O_{12}$ $Ir^{4+}_3O_{12}$

S_{trimer}:   1/2   0   0   1/2
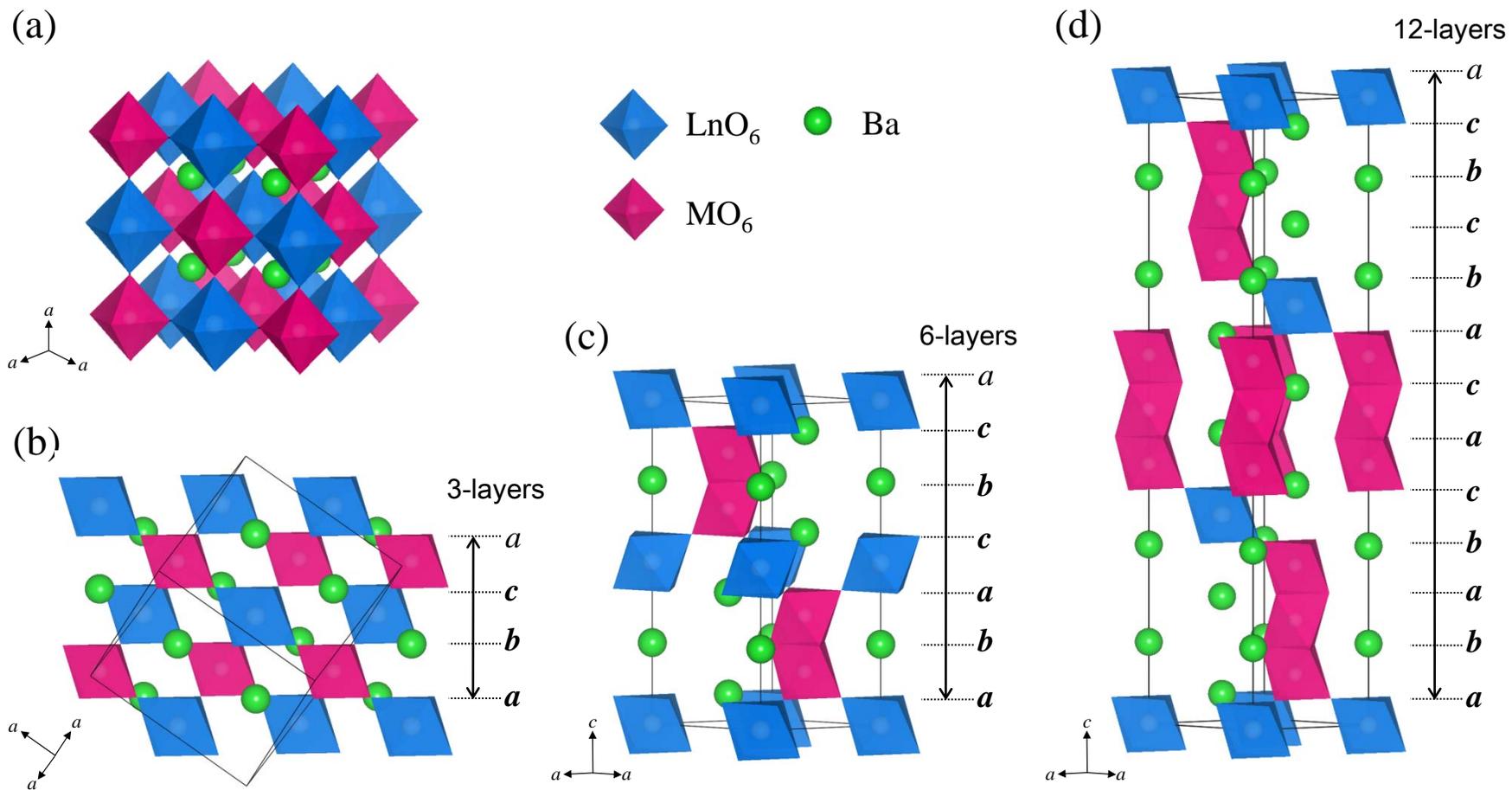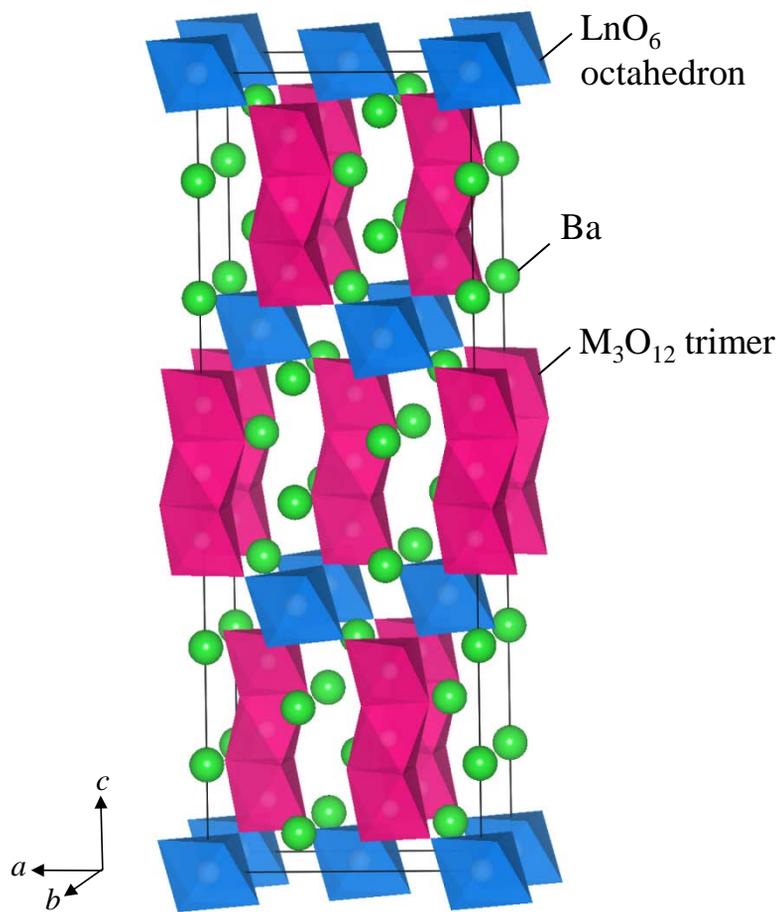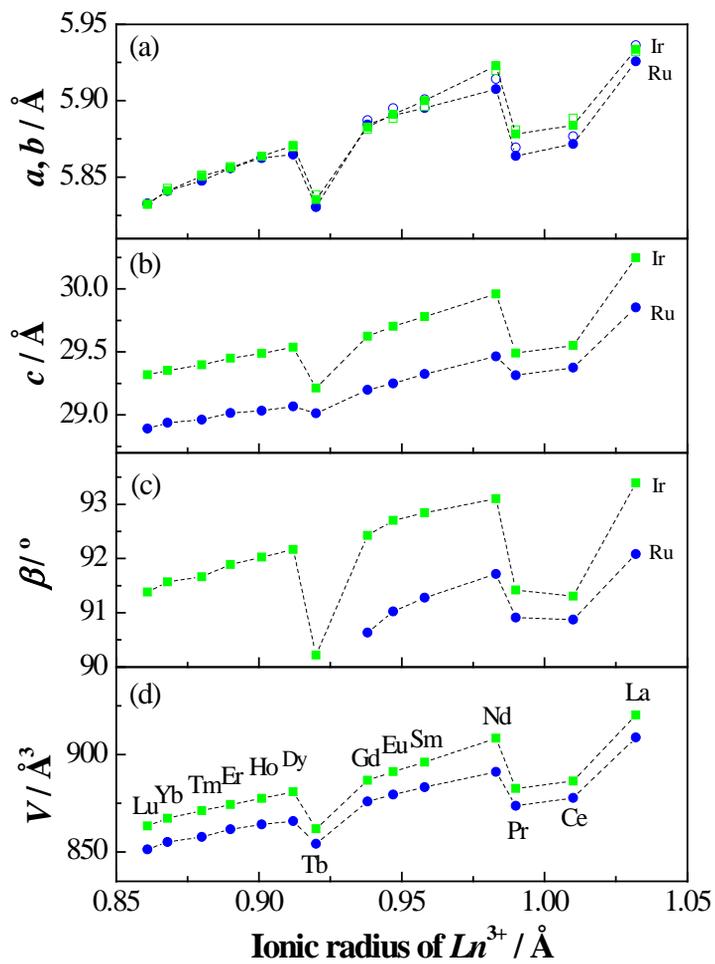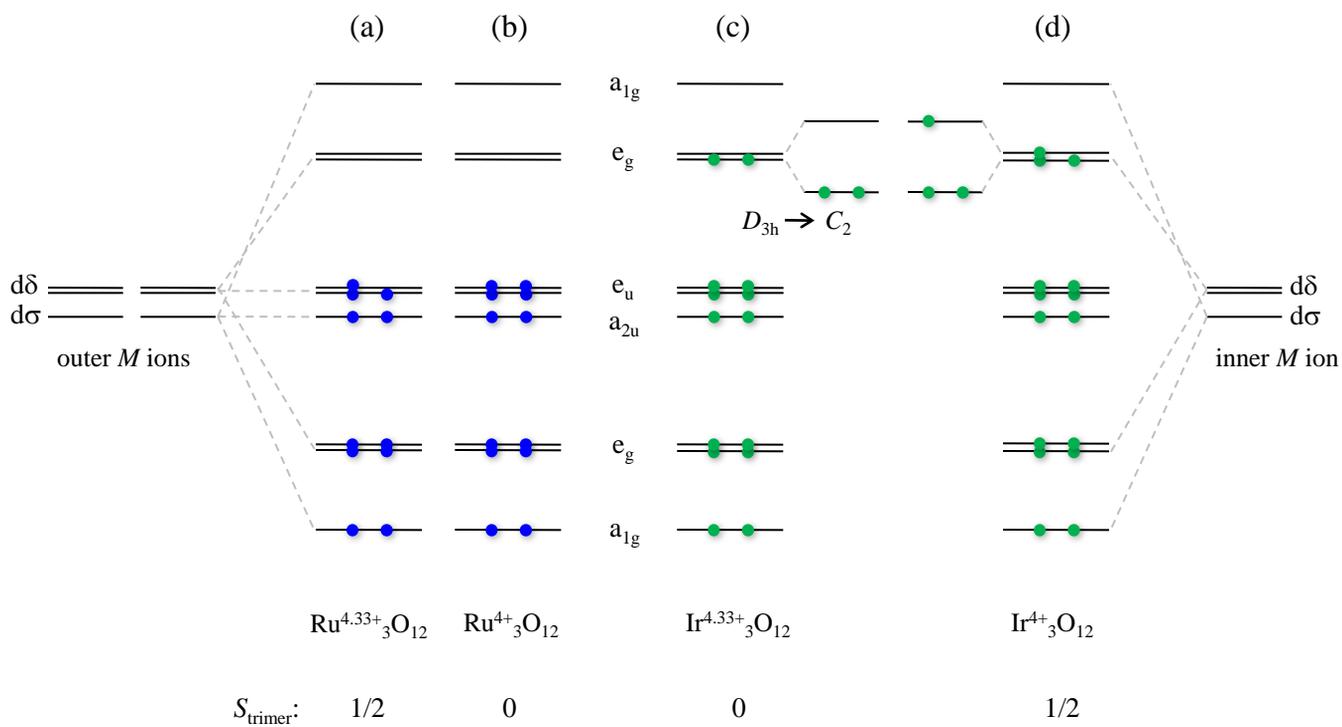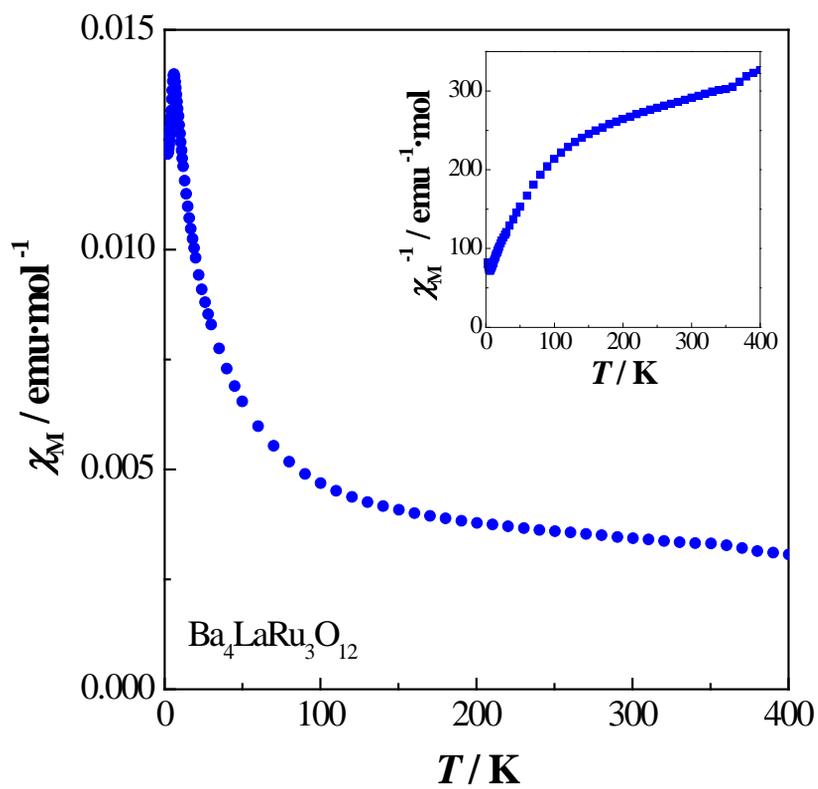
Fig. 5
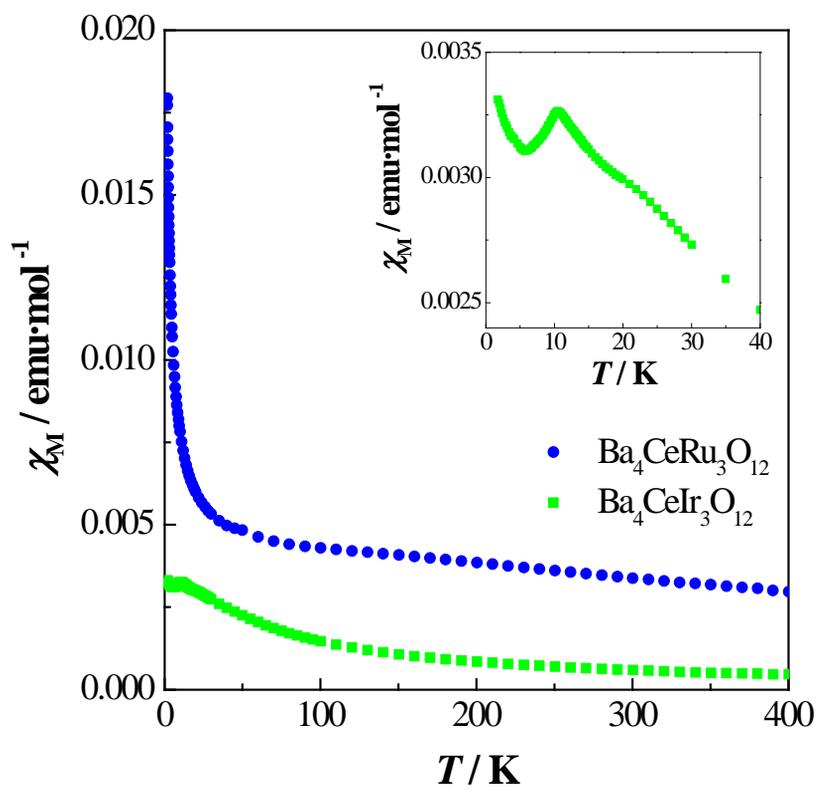
Fig. 6

Fig. 7

Fig. 8

Fig. 9

Fig. 10

(a)

T / K

1000 900 800 700 600 500 400

ρ / Ωcm

T^{-1} / 10^{-3} K^{-1}

(b)

T / K

300 200 100

ρ / Ωcm

$Ba_4EuIr_3O_{12}$

$Ba_4EuRu_3O_{12}$

$T^{-1/3}$ / $K^{-1/3}$